Supporting Information for

Self-enhanced peroxidase-like activity in a wide pH range enabled by heterostructured Au/MOFs nanozymes for multiple ascorbic acid-related bioenzymes analysis

Wendong Liu [a,#], Dingding Zhang [a,#], Fanghua Zhang [a], Zhe Hao [a], Yuyan Li [a], Mingzheng Shao [a], Ruizhong Zhang [a], Xiyan Li [b]*, Libing Zhang [a]**

[a] Tianjin Key Laboratory of Molecular Optoelectronic Sciences, Department of Chemistry, Tianjin University, Tianjin 300072 P. R. China

[b] Institute of Photoelectronic Thin Film Devices and Technology, Solar Energy Conversion Center, Key Laboratory of Photoelectronic Thin Film Devices and Technology of Tianjin, Engineering Research Center of Thin Film Photoelectronic Technology of Ministry of Education, Nankai University, Tianjin 300350 P. R. China

[#]Contributed equally.

*Corresponding author.

E-mail: zhangrz2019@tju.edu.cn (R.Z.); xiyan.li@nankai.edu.cn (X.L.); libing.zhang@tju.edu.cn (L.Z.)

Materials and methods

Reagents and materials. $HAuCl_4$, CH_3COOH, CH_3COONa, 1,2-diaminobenzene (OPD), 2,2'-azino-bis(3-ethylbenzothiazoline-6-sulfonic acid) (ABTS), Acarbose Hydrate were purchased from Shanghai Aladdin Biochemical Technology Co., Ltd. Alkaline phosphatase (ALP), sodium L-ascorbyl-2-phosphate (AAP), ascorbic acid oxidase (AAO) were purchased from Shanghai Maclin Biochemical Technology Co., Ltd. α-Glucosidase was purchased from Beijing Biotopped Technology Co., Ltd. Sodium hydrogen phosphate dihydrate, sodium dihydrogen phosphate anhydrous were purchased from Sun Chemical Technology (Shanghai) Co., Ltd. 3,3',5,5'-tetramethylbenzidine (TMB) was obtained from Shanghai Adamas Reagent Co., Ltd. Ultrapure water (≥18 MΩ, Millipore) was used in all experiments.

Instrumentation. The scanning electron microscopy (SEM) images were conducted using a Hitachi SU8010 scanning electron microscope. Transmission electron microscopy (TEM) measurements were made on a HITACHI H-8100 EM with an accelerating voltage of 200 kV. Autosorb-IQ analyzer was used for the Brunauer–Emmett–Teller (BET) surface area of the samples. All the Ultraviolet-visible (UV–vis) absorption spectra were obtained using UV756CRT (China).XPS measurement was performed on an ESCALAB-MKII spectrometer (VG Co., United Kingdom) with Al Kα X-ray radiation as the X-ray source for excitation. Powder X-ray diffraction (PXRD) patterns were obtained using a Rigaku Smart Lab. Fourier infrared spectra (FTIR) were recorded on Nicolet is5 (Thermo, USA). Inductively coupled plasma mass spectrometry (ICP-MS) measurements were performed on Agilent 725 (USA) to study the loading of Au in Au/UiO-66 according to the following formula:

$$C_x(mg/kg) = \frac{C_0(mg/L) * f * V_0(mL) * 10^{-3}}{m_0(g) * 10^{-3}} = \frac{C_1(mg/L) * V_0(mL) * 10^{-3}}{m_0(g) * 10^{-3}}$$

$$W(\%) = \frac{C_x(mg/kg)}{10^6} * 100\%$$

m_0: the quality of samples; V_0: volume after digestion; f: dilution ratio; C_o: the concentration of Au (mg/L); C_1: concentration of Au in the stock solution of sample digestion solution (mg/L); C_x: test result of Au concentration (mg/kg).

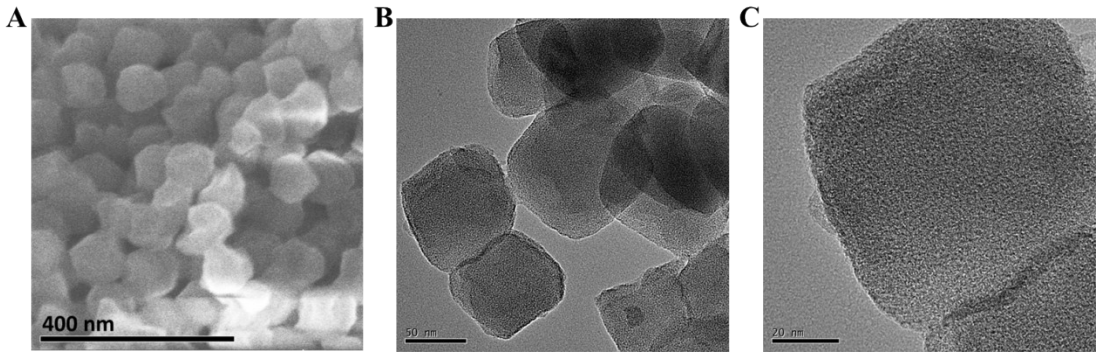

Fig. S1. SEM and TEM images of UiO-66 particles. (A) SEM image. (B, C) TEM images.

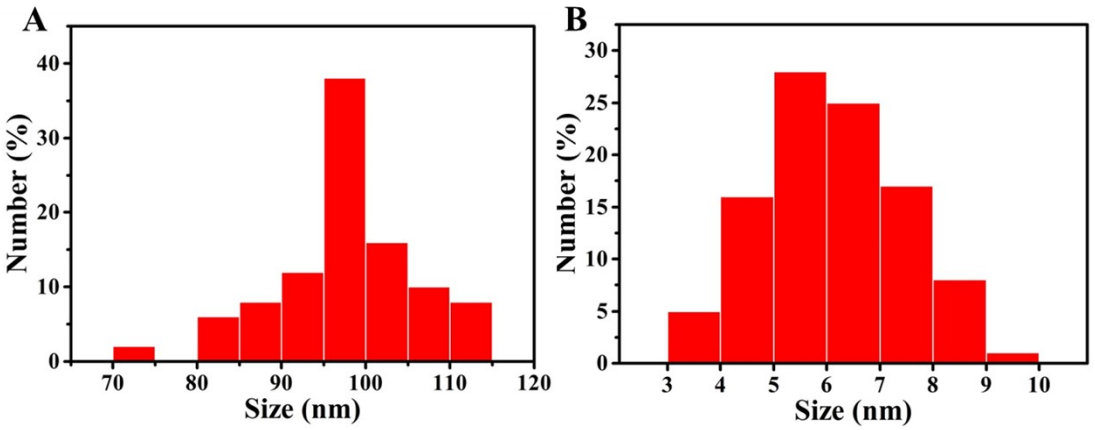

Fig. S2. Particle size distribution. (A) UiO-66 particles. (B) Au NPs attached on UiO-66 (1.8 wt %). (C)

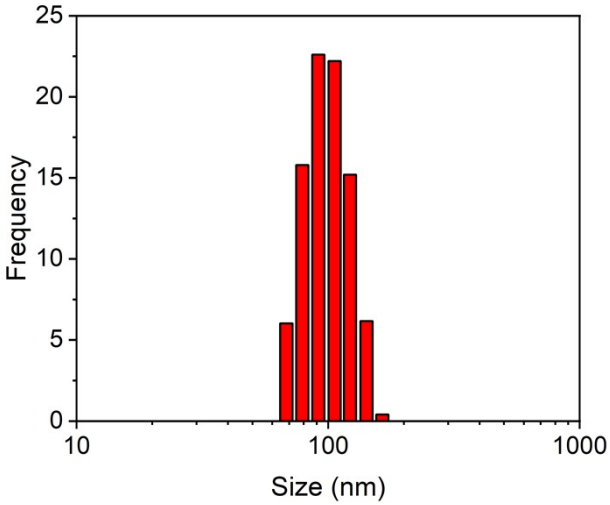

Fig. S3. Size distribution of Au NPs/UiO-66 (1.8 wt.% Au) characterized by dynamic light scattering (DLS). The DLS measurement shows that the hydrodynamic size of Au NPs/UiO-66 is approximately 100 nm.

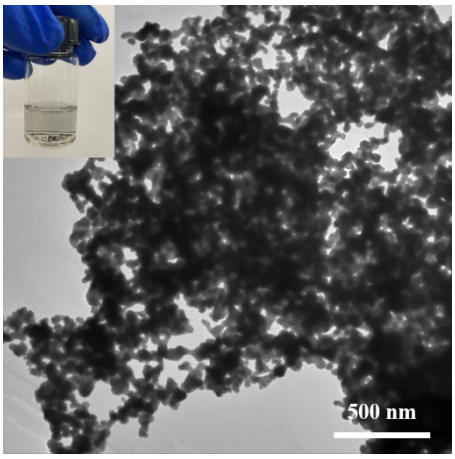

Fig. S4. TEM images of Au NPs.

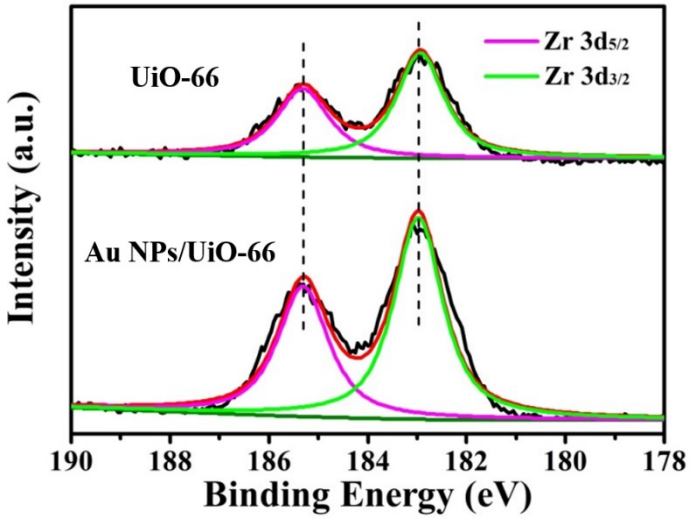

Fig. S5. High-resolution XPS spectra of Zr 3*d* in UiO-66 and Au NPs/UiO-66 particles.

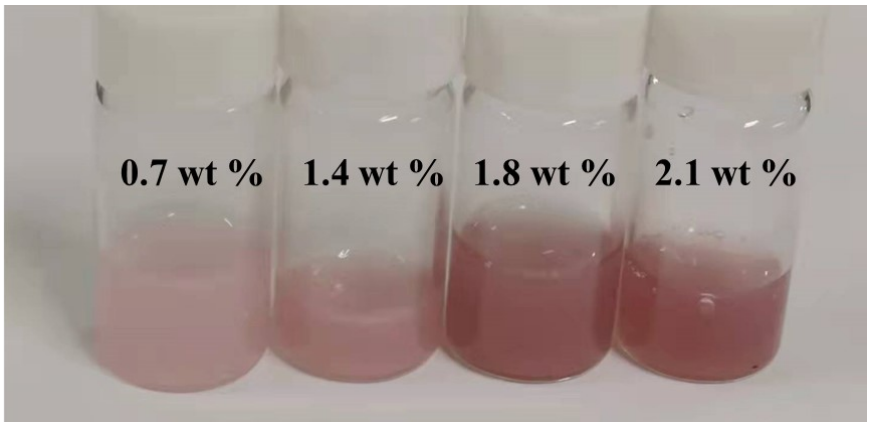

Fig. S6. Digital photograph for the aqueous dispersions (2 mg mL^{-1}) of Au NPs/UiO-66 particles with different Au mass loadings based on the ICP-MS results.

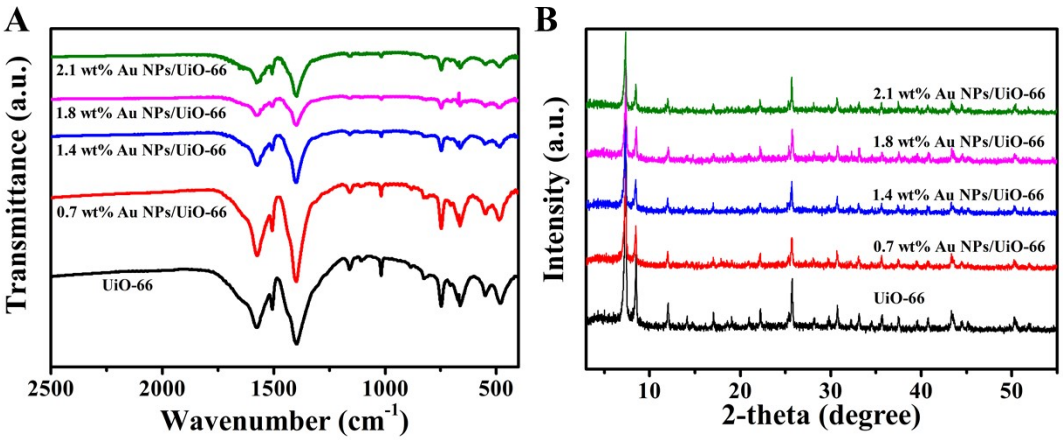

Fig. S7. Characterization of the Au NPs/UiO-66 particles with different Au mass loadings. (A) FTIR spectra and (B) PXRD patterns for Au NPs/UiO-66 particles with different Au mass loadings.

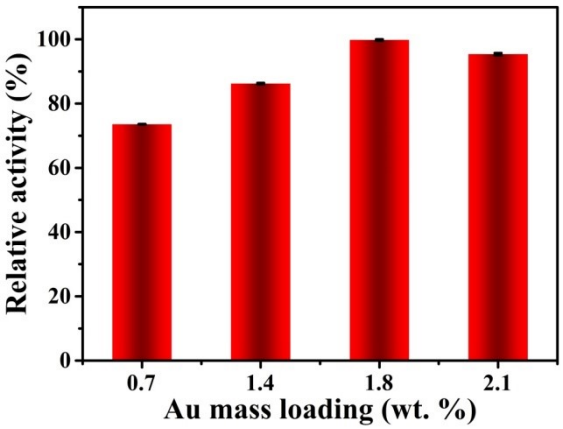

Fig. S8. The relative activity of different AuNPs/UiO-66 when the reaction content of Au is the same.

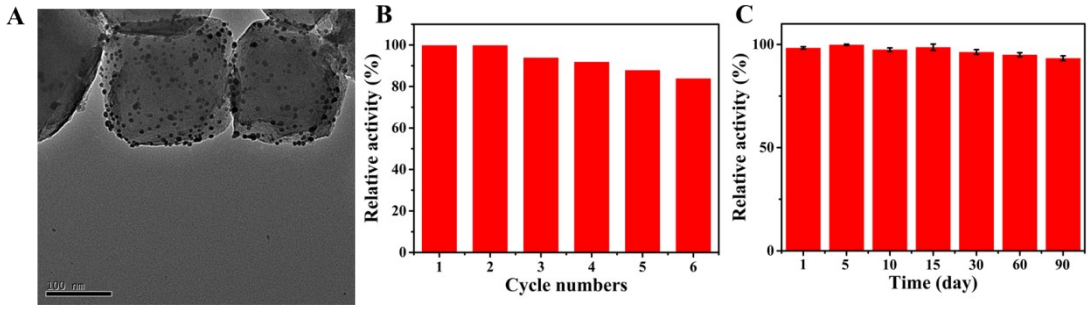

Fig. S9. Reusability and stability of Au NPs/UiO-66 nanozyme. (A) TEM image of Au NPs/UiO-66 nanozyme after 6 times of reaction with TMB in the presence of H_2O_2. (B) The relative activity of Au NPs/UiO-66 nanozyme for 6 consecutive cycles. (C) The relative activity of Au NPs/UiO-66 nanozyme after storage for different times.

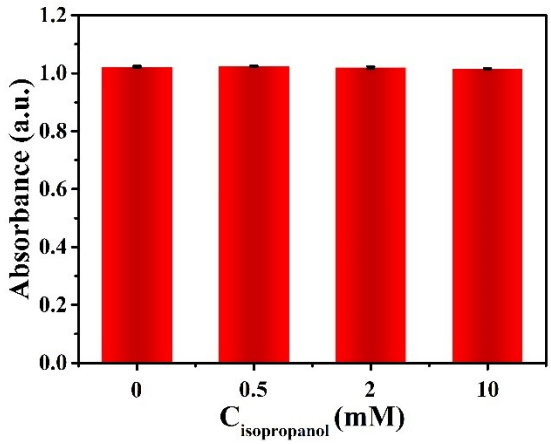

Fig. S10. The absorbance of ox-TMB under different concentrations of isopropanol. Reaction conditions: Au NPs/UiO-66 (0.1 mg mL^{-1}), H_2O_2 (25 mM), and TMB (0.5 mM) in acetate buffer (10 mM, pH 5.0).

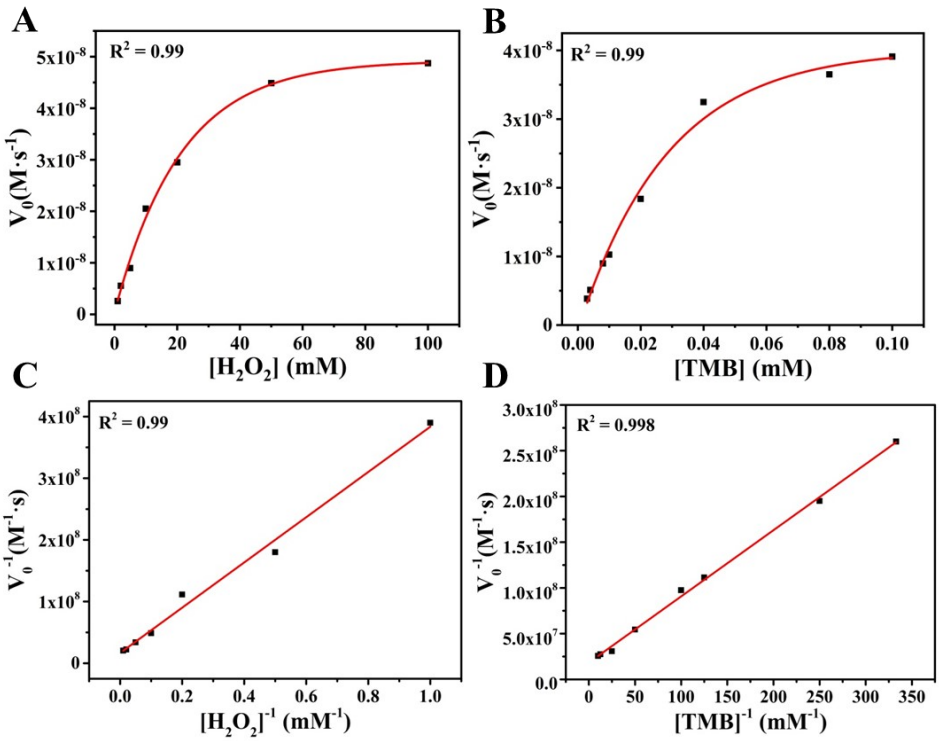

Fig. S11. Steady-state kinetic assay of Au NPs/UiO-66 nanozyme. (A) The reaction concentration of TMB (0.5 mM) remained the same and the velocity (λ_{Abs}=652 nm) varied with the concentration of H_2O_2, and (B) the reaction concentration of H_2O_2 (25 mM) remained the same and the velocity (λ_{Abs}=652 nm) varied with the concentration of TMB. Double reciprocal plots between velocity and(C) H_2O_2 concentration and (D) TMB concentration. Reaction condition: HAc-NaAc buffer (10 mM, pH 5.0), 0.1 mg mL^{-1} nanozyme.

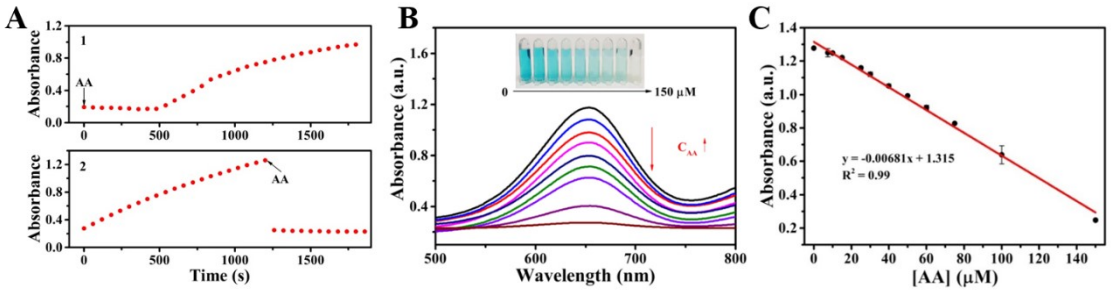

Fig. S12. Colorimetric response for AA assay. (A) Kinetic plots of A_{652} for Au NPs/UiO-66 catalyzed TMB oxidation in the presence of H_2O_2 and AA-medicated inhibitory effect on the peroxidase-like activity of Au NPs/UiO-66. (curve 1: Au NPs/UiO-66 + H_2O_2 + TMB + AA. curve 2: Au NPs/UiO-66 + H_2O_2 + TMB + AA, note: AA injection after 20 min incubation.). (B) UV-vis absorption spectra of the Au NPs/UiO-66-H_2O_2-TMB system with different concentrations of AA (0-150 μM). (C) Linear relationship between absorbance at 652 nm and concentrations of AA. Reaction conditions: pH 5, 25 mM H_2O_2, 0.5 mM TMB, 40 ℃, 0.1 mg mL^{-1} Au NPs/UiO-66 nanozyme.

Table S1. The surface areas and pore volumes of UiO-66 and Au@UiO-66 samples. The pore size model is "N_2 at 77 K on carbon (slit pore, NLDFT equilibrium model)".

Samples	Pore volume ($cm^3\ g^{-1}$)	Surface area ($m^2\ g^{-1}$)	Pore width (Mode) (nm)
UiO-66	0.521	922.4	0.822
Au NPs/UiO-66	0.442	783.1	0.785

Table S2. The mass loading of Au in Au NPs/UiO-66 particles at different concentrations of $HAuCl_4$.

$HAuCl_4$ (mM)	The load of Au in Au NPs/UiO-66 (wt %)
10	0.7
20	1.4
25	1.8
30	2.1

Table S3. Catalytic parameters comparison of Au NPs/UiO-66, HRP, and different Au-based catalysts.

Catalyst	Substrate	K_m (mM)	V_{max} (10^{-8} M·s^{-1})	[E] (mM)	K_{cat} (s^{-1})	Reference
HRP	H_2O_2	3.7	8.71	-		1
HRP	TMB	0.434	10	-		1
Tyr-Au NPs	H_2O_2	57.84	5.32	0.1	5.32×10^{-4}	2
Tyr-Au NPs	TMB	0.024	0.91	0.1	9.1×10^{-5}	2
citrate-Au NPs	H_2O_2	61.34	0.663	0.02	3.315×10^{-4}	3
citrate-Au NPs	TMB	0.11	1.539	0.02	7.695×10^{-4}	3
D-His@Au NCs	H_2O_2	72	5.55	-		4
D-His@Au NCs	TMB	0.41	7.69	-		4
BSA-Au NCs	H_2O_2	16.71	1.302	0.003	4.34×10^{-3}	5
BSA-Au NCs	TMB	3.59	0.861	0.003	2.87×10^{-3}	5
Au hydrogel	H_2O_2	19.92	12.8	-	-	6
Au hydrogel	TMB	0.32	12.30	-	-	6
ZnSA-AuAMP hydrogel	H_2O_2	30.53	1.679	-	-	7
ZnSA-AuAMP hydrogel	TMB	0.36	1.197	-	-	7
Au NPs/UiO-66	H_2O_2	21.915	5.974	0.005	0.012	This work
Au NPs/UiO-66	TMB	0.039	5.453	0.005	0.011	This work

[E] is the molar concentration of Au; K_{cat} is the catalytic constant, $K_{cat} = V_{max}/[E]$.

Table S4. Comparison of different optical α-Glu assays.

Materials	Mode	Linear range (U/mL)	LOD (U/mL)	Reference
Au NRs	Colorimetry	2.5-45	0.5	8
SA-Pt/CN	Colorimetry	0.01–8	0.0038	9
f-FeNC	Colorimetry	0.005–0.04, 0.04–0.1	0.00027	10
pAPG AuNPs	Colorimetry	0.05–1.1	0.04	11
CDs	Fluorometry	0.01–5.5	0.02	12
b-CDs	Fluorometry	0.13–6.7	0.036	13
F-PDA-CoOOH	Fluorometry	0.002–0.08	0.00165	14
PBA-CQD	Fluorometry	1.14–17.35	0.33	15
b-CDs	Fluorometry	0.13–6.7	0.036	13
AgInZnS QDs	Fluorometry	0.01–0.16	0.0073	16
Au NPs/UiO-66	Colorimetry	0.005-1.9	0.002	This work

Table S5. Comparison of different optical ALP assays.

Materials	Mode	Linear range (mU/mL)	LOD (mU/mL)	Reference
Fe/NC-SAs	Colorimetry	0.1-1.5	0.05	17
PB NCs	Colorimetry	0.6-6.0	0.23	18
Ir/LMIO	Colorimetry	0.39-100	0.39	19
Pd cube@CeO2	Colorimetry	0.1-4	0.07	20
Ag@Au NR	Colorimetry	2-20	0.53	21
Ferrocene-based substrate	Electrochemistry	1-1000	0.4	22
4-MPBAb-Au@Ag NPs	SERS	0.5-10	0.1	23
CdS QDs	Fluorimetry	0.2-30	0.2	24
b-CD/CQDs	Fluorometry	3.4–100	0.9	25
NB co-doped C-dots	Fluorometry	0.2–6.0	0.16	26
Au NPs/UiO-66	Colorimetry	1.25-37.5	0.14	This work

Table S6. Comparison of different optical ALP assays.

Materials	Mode	Linear range (mU/mL)	LOD (mU/mL)	Reference
C-dots	Colorimetry	0.04–8	0.012	27
Au/Ag NCs	Fluorometric	5-80	1.72	28
DNA-Au/Ag NC	Fluorimetry	10-200	4.8	29
MQDs	Fluorimetry	2-40	0.8	30
Carbon dots	Fluorimetry	0.04-5	0.017	27
Au NPs/UiO-66	Colorimetry	0.5-10	0.34	This work

References

1. Gao, L.; Zhuang, J.; Nie, L.; Zhang, J.; Zhang, Y.; Gu, N.; Wang, T.; Feng, J.; Yang, D.; Perrett, S.; Yan, X., Intrinsic peroxidase-like activity of ferromagnetic nanoparticles. *Nature Nanotechnology* **2007,** *2* (9), 577-583.

2. Weerathunge, P.; Ramanathan, R.; Torok, V. A.; Hodgson, K.; Xu, Y.; Goodacre, R.; Behera, B. K.; Bansal, V., Ultrasensitive Colorimetric Detection of Murine Norovirus Using NanoZyme Aptasensor. *Anal Chem* **2019,** *91* (5), 3270-3276.

3. Xue, Q.; Niu, X.; Liu, P.; Wang, M.; Peng, Y.; Peng, H.; Li, X., Analyte-triggered citrate-stabilized Au nanoparticle aggregation with accelerated peroxidase-mimicking activity for catalysis-based colorimetric sensing of arsenite. *Sensors and Actuators B: Chemical* **2021,** *334*.

4. Song, Y.; Qiao, J.; Liu, W.; Qi, L., Colorimetric detection of serum doxycycline with d-histidine-functionalized gold nanoclusters as nanozymes. *Analyst* **2020,** *145* (10), 3564-3568.

5. Hu, L.; Liao, H.; Feng, L.; Wang, M.; Fu, W., Accelerating the Peroxidase-Like Activity of Gold Nanoclusters at Neutral pH for Colorimetric Detection of Heparin and Heparinase Activity. *Anal Chem* **2018,** *90* (10), 6247-6252.

6. Jiao, L.; Xu, W.; Yan, H.; Wu, Y.; Gu, W.; Li, H.; Du, D.; Lin, Y.; Zhu, C., A dopamine-induced Au hydrogel nanozyme for enhanced biomimetic catalysis. *Chem. Commun.* **2019,** *55* (66), 9865-9868.

7. Liu, L.; Jiang, H.; Wang, X., Alkaline phosphatase-responsive Zn2+ double-triggered nucleotide capped gold nanoclusters/ alginate hydrogel with recyclable nanozyme capability. *Biosens. Bioelectron.* **2021,** *173*, 112786.

8. Cheng, X.; Huang, Y.; Yuan, C.; Dai, K.; Jiang, H.; Ma, J., Colorimetric detection of α-glucosidase activity based on the etching of gold nanorods and its application to screen anti-diabetic drugs. *Sens. Actuators, B* **2019,** *282*, 838-843.

9. Kang, G.; Liu, W.; Liu, F.; Li, Z.; Dong, X.; Chen, C.; Lu, Y., Single-atom Pt catalysts as oxidase mimic for p-benzoquinone and α-glucosidase activity detection. *Chem. Eng. J.* **2022,** *449*, 137855.

10. Zhang, C.; Chen, C.; Zhao, D.; Kang, G.; Liu, F.; Yang, F.; Lu, Y.; Sun, J., Multienzyme Cascades Based on Highly Efficient Metal–Nitrogen–Carbon Nanozymes for Construction of Versatile Bioassays. *Anal. Chem.* **2022,** *94* (8), 3485-3493.

11. Zhang, J.; Liu, Y.; Lv, J.; Li, G., A colorimetric method for α-glucosidase activity assay and its inhibitor screening based on aggregation of gold nanoparticles induced by specific recognition between phenylenediboronic acid and 4-aminophenyl-α-d-glucopyranoside. *Nano Res.* **2015,** *8* (3), 920-930.

12. Liu, Y.; Liu, W.-J.; Hu, J.; Li, Y.; Wang, Y.; Zhao, L.-X., Affinity binding-mediated

fluorometric protein assay based on the use of target-triggered DNA assembling probes and aptamers labelled with upconversion nanoparticles: application to the determination of platelet derived growth factor-BB. *Microchim. Acta* **2019,** *187* (1), 9.

13. Cheng, X.; Xu, J.; Wang, L.; Xu, G.; Wei, F.; Chai, Y.; Hu, Q.; Cen, Y., A redox modulated ratiometric fluorometric method based on the use of dual-color carbon dots for determination of the activity of enzymes participating in ascorbic acid-related reactions. *Microchim. Acta* **2019,** *186* (12), 818.

14. Zhang, H.; Wang, Z.; Yang, X.; Li, Z.-L.; Sun, L.; Ma, J.; Jiang, H., The determination of α-glucosidase activity through a nano fluorescent sensor of F-PDA−CoOOH. *Anal. Chim. Acta* **2019,** *1080*, 170-177.

15. Ao, H.; Feng, H.; Huang, X.; Zhao, M.; Qian, Z., A reversible fluorescence nanoswitch based on dynamic covalent B–O bonds using functional carbon quantum dots and its application for α-glucosidase activity monitoring. *Journal of Materials Chemistry C* **2017,** *5* (11), 2826-2832.

16. Zhang, J.; Liu, J.; Wang, M.; Wang, G.; Su, X., A fluorometric assay for α-glucosidase activity based on quaternary AgInZnS QDs. *Microchim. Acta* **2021,** *188* (7), 227.

17. Xie, X.; Wang, Y.; Zhou, X.; Chen, J.; Wang, M.; Su, X., Fe–N–C single-atom nanozymes with peroxidase-like activity for the detection of alkaline phosphatase. *Analyst* **2021,** *146* (3), 896-903.

18. Wu, T.; Hou, W.; Ma, Z.; Liu, M.; Liu, X.; Zhang, Y.; Yao, S., Colorimetric determination of ascorbic acid and the activity of alkaline phosphatase based on the inhibition of the peroxidase-like activity of citric acid-capped Prussian Blue nanocubes. *Microchim. Acta* **2019,** *186* (2), 123.

19. Jiang, X.; Wang, X.; Lin, A.; Wei, H., In Situ Exsolution of Noble-Metal Nanoparticles on Perovskites as Enhanced Peroxidase Mimics for Bioanalysis. *Anal. Chem.* **2021,** *93* (14), 5954-5962.

20. Wang, J.; Ni, P.; Chen, C.; Jiang, Y.; Zhang, C.; Wang, B.; Cao, B.; Lu, Y., Colorimetric determination of the activity of alkaline phosphatase by exploiting the oxidase-like activity of palladium cube@CeO2 core-shell nanoparticles. *Microchimica Acta* **2020,** *187* (2), 115.

21. Zhang, Q.; Yu, Y.; Yun, X.; Luo, B.; Jiang, H.; Chen, C.; Wang, S.; Min, D., Multicolor Colorimetric Sensor for Detection of Omethoate Based on the Inhibition of the Enzyme-Induced Metallization of Gold Nanorods. *ACS Applied Nano Materials* **2020,** *3* (6), 5212-5219.

22. Goggins, S.; Naz, C.; Marsh, B. J.; Frost, C. G., Ratiometric electrochemical detection of alkaline phosphatase. *Chem. Commun.* **2015,** *51* (3), 561-564.

23. Zhang, J.; He, L.; Zhang, X.; Wang, J.; Yang, L.; Liu, B.; Jiang, C.; Zhang, Z.,

Colorimetric and SERS dual-readout for assaying alkaline phosphatase activity by ascorbic acid induced aggregation of Ag coated Au nanoparticles. *Sens. Actuators B Chem.* **2017,** *253*, 839-845.

24. Malashikhina, N.; Garai-Ibabe, G.; Pavlov, V., Unconventional Application of Conventional Enzymatic Substrate: First Fluorogenic Immunoassay Based on Enzymatic Formation of Quantum Dots. *Anal. Chem.* **2013,** *85* (14), 6866-6870.

25. Tang, C.; Qian, Z.; Huang, Y.; Xu, J.; Ao, H.; Zhao, M.; Zhou, J.; Chen, J.; Feng, H., A fluorometric assay for alkaline phosphatase activity based on β-cyclodextrin-modified carbon quantum dots through host-guest recognition. *Biosens. Bioelectron.* **2016,** *83*, 274-280.

26. Ni, P.; Xie, J.; Chen, C.; Jiang, Y.; Lu, Y.; Hu, X., Fluorometric determination of the activity of alkaline phosphatase and its inhibitors based on ascorbic acid-induced aggregation of carbon dots. *Microchimica Acta* **2019,** *186* (3), 202.

27. Wang, Y.; Yang, Y.; Liu, W.; Ding, F.; Zou, P.; Wang, X.; Zhao, Q.; Rao, H., A carbon dot-based ratiometric fluorometric and colorimetric method for determination of ascorbic acid and of the activity of ascorbic acid oxidase. *Microchimica Acta* **2019,** *186* (4), 246.

28. Wang, M.; Wang, M.; Wang, G.; Su, X., A fluorescence "off–on–off" sensing platform based on bimetallic gold/silver nanoclusters for ascorbate oxidase activity monitoring. *Analyst* **2020,** *145* (3), 1001-1007.

29. Liu, S.; Pang, S., A dual-model strategy for fluorometric determination of ascorbic acid and of ascorbic acid oxidase activity by using DNA-templated gold-silver nanoclusters. *Microchimica Acta* **2018,** *185* (9).

30. Li, N.; Zhang, F.; Sun, W.; Zhang, L.; Su, X., Redox reaction-modulated fluorescence biosensor for ascorbic acid oxidase assay by using MoS2 quantum dots as fluorescence probe. *Talanta* **2021,** *222*, 121522.